On-demand erythrocyte disposal and iron recycling requires transient macrophages in the liver

HHS Public Access

Author manuscript

Nat Med. Author manuscript; available in PMC 2017 January 18.

Published in final edited form as:

Nat Med. 2016 August ; 22(8): 945–951. doi:10.1038/nm.4146.

On-demand erythrocyte disposal and iron recycling requires transient macrophages in the liver

Igor Theurl[1,2,3,#], **Ingo Hilgendorf**[1,2,4,#], **Manfred Nairz**[1,2,#], **Piotr Tymoszuk**[3], **David Haschka**[3], **Malte Asshoff**[3], **Shun He**[1,2], **Louisa M. S. Gerhardt**[1,2], **Tobias A. W. Holderried**[5], **Markus Seifert**[3], **Sieghart Sopper**[6], **Ashley M. Fenn**[1,2], **Atsushi Anzai**[1,2], **Sara Rattik**[1,2], **Cameron McAlpine**[1,2], **Milan Theurl**[7], **Peter Wieghofer**[8,9], **Yoshiko Iwamoto**[1,2], **Georg F. Weber**[1,2], **Nina K. Harder**[1,2], **Benjamin G. Chousterman**[1,2], **Tara L. Arvedson**[10], **Mary McKee**[1,11], **Fudi Wang**[12], **Oliver M. D. Lutz**[13], **Emanuele Rezoagli**[14], **Jodie L. Babitt**[1,11], **Lorenzo Berra**[14], **Marco Prinz**[8,15], **Matthias Nahrendorf**[1,2], **Guenter Weiss**[3], **Ralph Weissleder**[1,2,16], **Herbert Y. Lin**[1,11,*], and **Filip K. Swirski**[1,2,*]

[1]Center for Systems Biology, Massachusetts General Hospital and Harvard Medical School, Boston, MA, USA

[2]Department of Radiology, Massachusetts General Hospital and Harvard Medical School, Boston, MA, USA

[3]Department of Internal Medicine VI, Infectious Diseases, Immunology, Rheumatology, Pneumology, Medical University of Innsbruck, Innsbruck, Austria

[4]Heart Center Freiburg, University of Freiburg, Freiburg, Germany

[5]Department of Internal Medicine III, Oncology, Hematology and Rheumatology, University Hospital, Bonn, Germany

[6]Department of Internal Medicine V, Medical University of Innsbruck, Innsbruck, Austria

[7]Department of Ophthalmology and Optometry, Medical University of Innsbruck, Innsbruck, Austria

[8]Institute of Neuropathology, Freiburg University Medical Centre, Freiburg, Germany

[9]Faculty of Biology, University of Freiburg, Freiburg, Germany

[*]Correspondence: F.K.S. (fswirski@mgh.harvard.edu) or H.Y.L. (Lin.Herbert@mgh.harvard.edu).
[#]authors contributed equally

Accession codes

Genome-wide expression data were deposited in the GEO repository (GSE77106).

Author contributions

I.T., I.H., M.N. conceived the project, designed and performed experiments, analyzed and interpreted data, and wrote the manuscript; P.T., D.H., M.A., S.H., L.M.S.G., T.A.W.H., M.S., S.S., A.M.F., A.A., S.R., C.M., M.T., P.W., Y.I., G.F.W., N.K.H., B.G.C., M.M. performed experiments; T.L.A., F.W., M.P., P.W. provided materials and intellectual input; O.M.D.L., J.L.B., M.Nahrendorf, G.W. provided intellectual input and edited the manuscript; L.B. and E.R. conceived and conducted the clinical trial. R.W. edited the manuscript; H.Y.L. conceived the project, helped interpret data, and edited the manuscript; F.K.S. conceived the project, designed experiments, analyzed and interpreted data, and wrote the manuscript.

Competing financial interests: The authors declare no financial interests.

[10]Department of Oncology, Amgen Inc., Thousand Oaks, CA, USA

[11]Program in Membrane Biology, Division of Nephrology, Massachusetts General Hospital, Boston, MA, USA

[12]Department of Nutrition, Nutrition Discovery Innovation Center, Institute of Nutrition and Food Safety, School of Public Health, School of Medicine, Zhejiang University, Hangzhou, Zhejiang, China

[13]Austrian Drug Screening Institute, Innsbruck, Austria

[14]Department of Anaesthesia, Critical Care and Pain Medicine, Massachusetts General Hospital and Harvard Medical School, Boston, MA, USA

[15]BIOSS Centre for Biological Signalling Studies, University of Freiburg, Freiburg, Germany

[16]Department of Systems Biology, Harvard Medical School, Boston, MA, USA

Abstract

Iron is an essential component of the erythrocyte protein hemoglobin and is crucial to oxygen transport in vertebrates. In the steady state, erythrocyte production is in equilibrium with erythrocyte removal[1]. In various pathophysiological conditions, however, erythrocyte life span is severely compromised, which threatens the organism with anemia and iron toxicity[2,3]. Here we identify an on-demand mechanism that clears erythrocytes and recycles iron. We show that Ly-6C^{high} monocytes ingest stressed and senescent erythrocytes, accumulate in the liver via coordinated chemotactic cues, and differentiate to ferroportin 1 (FPN1)-expressing macrophages that can deliver iron to hepatocytes. Monocyte-derived FPN1^{+} Tim-4^{neg} macrophages are transient, reside alongside embryonically-derived Tim-4^{high} Kupffer cells, and depend on Csf1 and Nrf2. The spleen likewise recruits iron-loaded Ly-6C^{high} monocytes, but these do not differentiate into iron-recycling macrophages due to the suppressive action of Csf2. Inhibiting monocyte recruitment to the liver leads to kidney and liver damage. These observations identify the liver as the primary organ supporting rapid erythrocyte removal and iron recycling and uncover a mechanism by which the body adapts to fluctuations in erythrocyte integrity.

The physiological 120 day lifespan of human erythrocytes (i.e., red blood cells, RBC)[4,5] is shortened in various pathologies[6–10]. Red blood cell production requires a sufficient supply of iron: when iron stores are low, erythrocytes cannot be produced efficiently, causing anemia and tissue hypoxia. Because iron is poorly acquired through diet, most of the daily amount needed for erythropoiesis is recycled by the reticuloendothelial system in the spleen and liver in a process that depends on the transmembrane iron export protein ferroportin-1 (FPN1)[1,11,12]. Disease-borne erythrocyte damage threatens the organism in several ways: (i) damaged erythrocytes release hemoglobin and heme, which can cause acute kidney injury; (ii) erythrocyte loss leads to anemia; and (iii) the heightened need for erythrophagocytosis may overwhelm physiologic erythrocyte-clearing capacities, thereby liberating vast quantities of iron, which, although essential to life, is toxic in its non-transferrin-bound form[1]. We therefore hypothesized that vertebrate animals have evolved mechanisms that can adapt to fluctuations in erythrocyte integrity.

Erythrocytes and leukocytes can be identified as Ter119^{+} CD45^{-} and Ter119^{-} CD45^{+} cells, respectively (Supplementary Fig. 1a). Labeling erythrocytes with a membrane-integrating dye (pkh26) *ex vivo* allowed for *in vivo* detection and tracking (Fig. 1a). Whereas most "young" erythrocytes circulated in host blood for at least 16 h, aged and stressed erythrocytes[13,14]) quickly disappeared (Supplementary Fig. 1b). Stressed erythrocytes co-localized with leukocytes predominantly in the liver (Fig. 1b), but also the spleen, bone marrow, blood, and lung. Although splenectomized mice had higher percentages of delivered erythrocytes in the circulation compared to non-splenectomized controls, near-complete hepatectomy (95%) resulted in pronounced erythrocyte persistence in the circulation, while combined splenectomy and near-complete hepatectomy had the greatest effect on the persistence of damaged RBC in the blood (Fig. 1c, d and Supplementary Fig. 2a).

In the steady state, the liver contains abundant F4/80^{high} CD11b^{int} Kupffer cells (KC) and relatively few CD11b^{high} cells (Fig. 1e). Stressed erythrocyte challenge led to dramatic leukocyte fluctuations in the liver. At 3 h, monocyte numbers peaked (Figure 1f). At 16 h, a population of CD11b^{high} F4/80^{high} macrophages (henceforth called transient macrophages [tMΦ]) appeared (Fig. 1e, f), but F4/80^{high} CD11b^{int} KC diminished. At 72–168 h the populations returned to near-basal levels (Fig. 1e, f). The spleen, which contains F4/80^{high} CD11b^{int} red pulp macrophages (RPM) and monocytes, accumulated monocytes, but hardly any tMΦ, after stressed erythrocyte challenge (Fig. 1e, f). The phenomenon was specific to hemoglobin-containing erythrocytes as injecting hemoglobin-depleted "ghosts" did not induce the appearance of tMΦ (Fig. 1e).

We used two independent approaches to track sRBC uptake by leukocytes. First, flow cytometry and histology detected pkh26 fluorescence on gated and sorted leukocyte populations, respectively, as a surrogate for sRBC ingestion (Supplementary Figs. 2b–d and 3). In the blood, Ly-6C^{high} monocyte ingestion of sRBC peaked 1 h after challenge and sRBC-laden monocytes (Supplementary Fig. 4a) subsequently accumulated in the liver and spleen (Supplementary Fig. 4b, c). At 16 h, tMΦ in the liver contained the largest proportion of stressed erythrocytes (Fig. 1g and Supplementary Fig. 4b, c). No tMΦ appeared in the spleen, bone marrow, kidney, or lung (Supplementary Fig. 4d). Immunofluorescence substantiated these observations (Fig. 1h and Supplementary Fig. 2b, c). Second, we measured iron content in sorted leukocytes by atomic absorption spectroscopy, and confirmed that tMΦ in the liver contained the bulk of the iron (Fig. 1i) because of abundant sRBC ingestion, likely via scavenger receptors such as SR-A and CD36 (Supplementary Fig. 5a–b)[15]. The spleen was dispensable to the appearance of tMΦ in the liver (Supplementary Fig. 5c), while lethal irradiation, which depleted monocytes without affecting KC or RPM at 10 d, impaired erythrocyte clearance (Supplementary Fig. 5d–f).

Shortly after stressed erythrocyte challenge, we detected erythrophagocytosing macrophages by scanning electron microscopy (Fig. 1j) and observed a punctate pattern of iron stores that was consistent with confinement in macrophages (Supplementary Fig. 6a). By 1 week, however, iron was stored in hepatocytes, giving rise to a diffuse parenchymal accumulation pattern. Quantifying iron distribution showed the greatest increase in the liver, as well as enhanced hepatocyte-derived hepcidin (Supplementary Fig. 6b)[1,4,16]. Using a model of hemolytic anemia involving phenylhydrazine (PHZ) delivery[17,18], anemia of inflammation

induced by heat-inactivated *Brucella abortus*[19,20], and a model of sickle cell anemia[21], we likewise detected tMΦ accumulation in the liver, but not spleen (Supplementary Fig. 7). In humans, erythrocyte damage resulted in erythrocyte accumulation in circulating classical monocytes along with higher intracellular and serum iron levels (Supplementary Fig. 8).

Macrophage-ingested iron is either stored in the cytoplasm or is exported via FPN1[11]. The spleen and liver expressed Ferritin and FPN1 in the steady state (Supplementary Fig. 9a–c), as expected[17,18]. Among the leukocytes, KC and RPM expressed FPN1 on their surfaces (Fig. 2a) for iron transport (Supplementary Fig. 9d). However, transfusing stressed iron-containing erythrocytes amplified FPN1 in the liver, but not the spleen (Fig. 2a and Supplementary Fig. 9a–c), and intensified FPN1 surface expression on tMΦ specifically in the liver (Fig. 2a). The abundant appearance of tMΦ required intact stressed erythrocytes (Supplementary Fig. 9e) and was exacerbated in response to competitive inhibition of the heme-cleaving enzyme heme-oxygenase (Hmox) 1 by tin-protoporphyrin IX (SnPP-IX) (Supplementary Fig. 9f). These results suggest that the liver is uniquely mechanistically equipped to respond to increased demand for erythrophagocytosis.

Given the phenotypic similarities between monocytes and tMΦ, we tested whether Ly-6C^{high} monocytes give rise to FPN1^{+} tMΦ in the liver. We adoptively transferred GFP^{+} Ly-6C^{high} and Ly-6C^{low} monocytes to animals receiving stressed erythrocytes. Immediately after transfer, both monocyte subsets circulated in the blood, but neither produced FPN1 (Fig. 2b). 16 h later, Ly-6C^{high} monocytes with augmented F4/80 appeared in the liver, thus resembling tMΦ (Fig. 2b). By 72 h, these Ly-6C^{high} monocyte-derived tMΦ further differentiated to resemble KC; they still contained erythrocytes (or their remnants), and they still expressed FPN1 and classical macrophage signature proteins,[22] MerTK and CD64, on their surfaces (Fig. 2b). In contrast, Ly-6C^{low} monocytes infiltrated the liver in lower numbers, did not differentiate to tMΦ, and remained FPN1^{-}, MerTK^{-}, and CD64^{-} (Fig. 2b and Supplementary Fig. 9g). Moreover, monocyte-to-FPN1^{+} macrophage differentiation was specific to the liver, and only a few of the transferred cells from either subset accumulated in the spleen (Fig. 2b). We observed a similar phenomenon by transfering GFP^{+} Ly-6C^{high} monocytes to the chronic sickle-cell disease model (Supplemetary Fig. 10a–b).

To test whether Ly-6C^{high} monocytes can support long-term KC renewal or whether KC ultimately remain tissue-derived, we joined C57BL/6 and GFP^{+} mice by parabiosis (Supplementary Fig. 10c–d)[23]. In the absence of erythrocyte delivery, Ly-6C^{high} blood monocyte chimerism rose to ~25% in the first 2 weeks and remained unchanged for >100 days, while KC chimerism remained low at <2% for the duration of the experiment (Fig. 2c). Erythrocyte delivery 2 weeks after parabiosis began had no effect on blood monocyte chimerism, but magnified chimerism among KC for >28 days (Fig. 2c). In contrast, RPM chimerism in the spleen did not respond to erythrocyte challenge. The data show that a high demand for erythrophagocytosis mobilizes erythrocyte-ingesting Ly-6C^{high} monocytes to the liver where they first differentiate to iron-recycling tMΦ and then to iron-recycling Kupffer-like cells. When demand declines, monocyte-derived KC-like cells disappear, and the remaining KC replenish independently of monocytes or other circulating progenitors.

To dig deeper into how monocyte and tissue-derived macrophages differ, we first sorted erythrocyte^{+} and erythrocyte^{-} liver KC and tMΦ 16 h after erythrocyte challenge. We then profiled gene expression by RT-PCR (Fig. 2d) and flow cytometry (Supplementary Fig. 10e), detecting numerous differences, including in SPI-C expression[17,18]. Next, we performed formal lineage tracing experiments because increased KC chimerism after erythrocyte challenge (Fig. 2c), along with tMΦ's shift to the KC gate, indicated that, for a limited time after challenge, KC are a mixed population comprising tissue and blood-derived cells. We used Cx3cr1-CreERT2 females mated with *ROSA26-tdTomato*$^{fl/fl}$ (*R26-tdT*) males[24,25], which, in the Cx3cr1-CreERT2 R26-tdT pups, gave rise to tdT^{+} KC and tdT^{-} monocytes (Fig. 2e). On day P70, we transplanted GFP^{+} bone marrow to generate GFP^{+} monocytes in the grown pups (Fig. 2e and Supplementary Fig. 11a). On day P91, we challenged the mice with stressed erythrocytes and, 7 days later, detected (embryonic, eKC) tdT^{+} GFP^{-} and (monocyte-derived, mKC) tdT^{-} GFP^{+} macrophages inside the KC gate. We then sorted these cells for microarray analysis (Fig. 2e). Our data showed numerous differences between the cells (Fig. 2f and Supplementary Fig. 11b), although iron metabolism mediators were comparable (Supplementary Fig. 11b, c). Among the differentially-expressed genes, *Timd4*, which produces the surface Tim-4 protein, was highly expressed in embryonic but not monocyte-derived KC (Fig. 2f), which we confirmed by flow cytometry (Fig. 2g). These data show that as tMΦ temporarily shift to the KC gate, they nevertheless differ from their embryonically derived counterparts.

The growth factors colony stimulating factor (Csf)-1 and Csf2 instruct myeloid cell fate decisions[26,27]. Following erythrocyte challenge, the liver and spleen augmented *Csf1* (Fig. 3a), the spleen but not liver augmented *Csf2* expression (Fig. 3b), the lung augmented neither (Supplementary Fig. 12a), and the bone marrow augmented *Csf2* (Supplementary Fig. 12b). Consequently, the liver had a high *Csf1*-to-*Csf2* ratio whereas the spleen and bone marrow had a low *Csf1*-to-*Csf2* ratio (Fig. 3c and Supplementary Fig. 12b) after stressed erythrocyte injection. To evaluate whether the growth factors cultivate the selective appearance of iron recycling macrophages, we first performed *in vitro* experiments. Ly-6C^{high} monocytes (Fig. 3d) – and their human counterparts, CD14^{high} CD16^{-} monocytes (Fig. 3e) – cultured in a Csf1-rich environment amplified FPN1 in response to sRBC, while culture with Csf2 suppressed it (Fig. 3f). This antagonism was specific to monocytes, as cultured RPM retained FPN1 in the presence of Csf2 (Supplementary Fig. 12c). KC were the dominant source of Csf1 *in vivo* (Supplementary Fig. 12d) and Csf1-driven FPN1 augmentation was specific to Ly-6C^{high} when compared to Ly-6C^{low} monocytes (Supplementary Fig. 12e).

Nuclear factor, erythroid derived 2, like 2 (Nrf2) recognizes heme groups and facilitates FPN1 transcription[28,29]. In the absence of Nrf2, Csf1 failed to stimulate FPN1 production on Ly-6C^{high} monocytes, which indicates that Csf1-dependent FPN1 enhancement requires Nrf2 (Fig. 3g). To confirm this *in vivo*, we delivered erythrocytes into either wild type mice receiving a Csf1 inhibitor or to *Nrf2*$^{-/-}$ mice. In both cases, FPN1^{+} tMΦ failed to arise in the liver despite the appearance of F4/80^{high} and CD11b^{high} cells (Fig. 3h). FPN1 expression on Kupffer cells likewise required Nrf2 but, unlike tMΦ, remained unaffected by Csf1 blockade. To determine whether Csf2 suppressed the appearance of tMΦ *in vivo*, we also delivered erythrocytes into *Csf2*$^{-/-}$ mice. In the absence of Csf2, FPN1^{+} tMΦ appeared in

the spleen, concomitant with augmented iron metabolism mediators (Supplementary Fig. 13). These data show that Nrf2 and Csf1 guide the production and maintenance of iron recycling macrophages in the liver, while Csf2 antagonizes iron recycling in the spleen under stress.

Because the liver selectively accumulated monocyte-derived tMΦ, we surmised that chemokines were guiding monocytes to this organ. The chemokines Ccl2 and Ccl3 (Fig. 4a) strongly responded to erythrocyte delivery in the liver but not the spleen, while expression of Ccl21 was curtailed in the spleen but not the liver (Supplementary Fig. 14). Differences among other chemokines were less pronounced (Supplementary Fig. 14a). Injecting Ccr2 and Ccr5 antagonists in conjunction with stressed erythrocyte delivery reduced Ly-6C^{high} monocyte and tMΦ populations in the liver but not the spleen or blood while increasing monocytes in the bone marrow (Fig. 4b), indicating impaired monocyte mobilization and recruitment. Accordingly, the antagonists boosted the number of circulating stressed erythrocytes in the blood, signaling impaired clearance (Fig. 4c).

Using this method, we discovered that interfering with on-demand monocyte recruitment increased enanched labile plasma iron (eLPI) (Fig. 4d), suggesting that impaired clearance of stressed erythrocytes by monocyte-derived tMΦ leads to the build-up in the circulation of tissue-damaging iron, heme, and hemoglobin. In support of this, we detected heightened production of haptoglobin and hemopexin in the liver (Fig. 4e) and higher levels of alanine aminotransferase (ALT), aspartate aminotransferase (AST), amylase, and blood urea nitrogen (BUN) (Fig. 4f). The number of tMΦ in the liver inversely correlated with eLPI, AST, and BUN (Supplementary Fig. 15). Moreover, blocking tMΦ accumulation in the liver led to increased iron deposition and nephron damage in the kidney following sRBC challenge (Fig. 4g and Supplementary Fig. 16a). We observed similar damage after Hmox1 blocking [30], PHZ-induced hemolysis, and in sickle cell disease (Supplementary Fig. 16b). Finally, the clinical manifestations of inadequately cleared stressed erythrocytes by FPN1^{+} tMΦ were phenocopied in mice whose monocyte-derived macrophages lacked FPN1 (Supplementary Fig. 17a–b)[31], and were ameliorated in a rescue experiment using LysM-specific FPN1-deficient mice (Supplementary Fig. 17c). These findings indicate that Ly-6C^{high} monocyte hepatic recruitment and differentiation to iron-recycling macrophages preserves organismal homeostasis during fluctuations of erythrocyte integrity.

In sum, we show that Ly-6C^{high} monocytes and their progeny propagate on-demand high-capacity erythrophagocytosis and iron recycling. This liver-specific phenomenon is transient, dynamic, requires cell-intrinsic and environmental triggers, and controls iron homeostasis during erythrocyte damage (Supplementary Fig. 18). Understanding and eventually harnessing this mechanism may help to treat persons with abnormally heightened erythrocyte elimination due to sepsis, various forms of inflammation, frequent blood transfusions, and inborn and acquired defects in erythrocyte stability.

Online Methods

Animals

C57BL/6J (wild type, WT), B6.SJL-*Ptprc*^{a} *Pepc*^{b}/BoyJ (CD45.1^{+}), C57BL/6-*Tg(UBC-GFP)30Scha*/J (*GFP*$^{+}$), B6.129X1-*Nfe2l2*^{tm1Ywk}/J (*Nrf2*$^{-/-}$), B6.Cg-*Msr1*^{tm1Csk}/J (*Msr1*$^{-/-}$), B6.129S1-*Cd36*^{tm1Mfe}/J (*CD36*$^{-/-}$), B6.129-*Hba*$^{tm1(HBA)Tow}$/*Hbb*$^{tm2(HBG1,HBB*)Tow}$ (sickle cell disease, SCD) and B6.129-*Hba*$^{tm1(HBA)Tow}$/*Hbb*$^{tm3(HBG1,HBB*)Tow}$ (non-sickling transgenic control, tgCtrl.) mice were purchased from The Jackson Laboratory (Bar Harbor, ME, USA). GM-CSF-deficient mice (*Csf2*$^{-/-}$) on a C57BL/6J background were bred in-house. B6.129S6-*Gt(ROSA)26Sor*$^{tm9(CAG-tdTomato)Hze}$/J (*ROSA26-tdTomato*$^{fl/fl}$ or *R26-tdT*) and B6.129P2(Cg)-B6.129P2(C)-*Cx3cr1*$^{tm2.1(cre/ERT2)Jung}$/J (*Cx3cr1-CreERT2*) [24,25] were kindly provided by Prof. Dr. M. Prinz. Mice carrying the myeloid-specific knockout of the FPN1 gene (*LysM*$^{Cre/+}$ *Slc40a1*$^{fl/fl}$) were kindly provided by Dr. F. Wang, back-crossed on a C57BL/6 background and bred in house. Unless otherwise indicated age- and sex-matched animals were used at 8 – 12 weeks of age. Where appropriate, animals were randomly assigned to interventions. All protocols were approved by the Animal Review Committee at Massachusetts General Hospital (Protocol No. 2011N000035 and 2015N000044) and by the Federal Ministry of Science, Research and Economy in Austria (Project No. BMWFW-66.011/0115-WF/V/3b/2014).

Erythrocyte preparation and pkh26 labeling

RBC preparation: Isolating, storing, and aging of red blood cells (RBC) from the blood of C57BL/6J WT mice was performed as described previously[13]. In detail, whole blood collected from C57BL/6J WT mice was pooled, centrifuged at 400 g for 10 min and the buffy coat was removed. In a second step RBC were diluted in PBS and further leukoreduced using a Neonatal High-Efficiency Leukocyte Reduction Filter (Purecell Neo, Pall Corporation). One part of RBC was placed in Eppendorf tubes and stored in the dark at 4 °C for 14 d (aged, aRBC) and another part was heated for 20 min at 48 °C while continuously shaking, generating stressed erythrocytes (stressed, sRBC). Naïve young erythrocytes (yRBC) were stored in the dark at 4 °C and delivered within 1 h of isolation. *Pkh26 labeling*: 1×10^{10} RBC were resuspended in 1 ml diluent C, mixed with 1 ml diluent C containing 4 μM PKH-26 (Sigma, St. Louis, MO, USA) and incubated for 5 min at RT in the dark before stopping the reaction by adding 10 ml PBS with 0.5% BSA and 2% FCS. After two washing steps with PBS, RBC were resuspended in PBS followed by a centrifugation step at 400 g for 15 min to reduce the volume to a final hemoglobin level ranging from 17.0 to 17.5 g/dl, as determined by HemaTrue (Heska, Loveland, CO, USA). The number of residual leukocytes was enumerated by HemaTrue and flow cytometry. Human RBC used for *in vitro* experiments were prepared exactly as described above for mouse RBC. *Ghost preparation:* RBC ghosts were obtained by hypotonic lysis of twice the volume of aged RBC as used for *in vivo* experiments (ie, for 100 μl of ghosts, 200 μl of aged RBCs were hemolyzed) with PBS to distilled water (1:15), followed by at least 5 washes with the same buffer and centrifugation at 30 g for 5 min until a white pellet was obtained. The pellet of RBC ghosts was resuspended in PBS and used for *in vivo* experiments.

Animal models and *in vivo* interventions

Hepatectomy and splenectomy: Lobectomy of liver tissue was performed after blood vessel ligation with 7-0 Ethilon suture. Removal of the left, median and caudate lobe (lobes 1–3) represented 70% liver resection. Removal of the left, median and right lateral lobe (lobes 2–5) represented 95% liver resection. Removal of the small caudate lobe (lobe 1) served as sham control (see Supplementary Fig. 2a). Spleens were removed with the use of electrocauterization. *Delivery of RBC*: RBC were isolated and adjusted to 17.5 g/dl hemoglobin as described above. 400 μl were injected i.v. per mouse. This amount of RBC delivery in mice corresponds to transfusion of two units of packed RBC in humans. *Ki20227 injection*: In some experiments the RBC transfer was accompanied by s.c. injection of the c-fms tyrosine kinase inhibitor Ki20227 at 50 mg/kg bodyweight (Tocris Biosciences, Bristol, UK). *DAPTA and RS504393 injection*: In some experiments the RBC transfer was accompanied by i.p injection of the Ccr2 antagonist RS504393 at 1 mg/kg bodyweight dissolved in DMSO (Tocris Biosciences, Bristol, UK) and the Ccr5 antagonist DAPTA at 2 mg/kg bodyweight (Tocris Biosciences, Bristol, UK) dissolved in sterile water. Both antagonists where administered again 6 h after sRBC transfer. *SnPP-IX injection*: In some experiments, the RBC transfer was accompanied by i.p injection of the heme-oxygenase (Hmox) 1 inhibitor tin-protoporphyrin IX (SnPP-IX) at 0.5 mg/kg bodyweight (Cayman Chemical, Ann Arbor, MI, USA). SnPP-IX was dissolved in 0.2 M NaOH and the pH was adjusted to 7.40 with 1 M HCl. SnPP-IX was administered every 8 h starting 30 min before sRBC transfer. *Irradiation:* In some experiments mice were lethally radiated (10 Gy) but not reconstituted with donor bone marrow cells for 10 d. *Adoptive transfer*: Ly-6C^{high} and Ly-6C^{low} monocytes were isolated by flow assisted cell sorting (FACS) from spleens or bone marrow of GFP^{+} mice and 1×10^{6} cells/mouse were injected i.v. followed by an additional sRBC injection. *Parabiosis*: Mice were joined in parabiosis as previously described[32]. In brief, the opposing lateral sides of mice were shaved, skin incisions made from behind the ear to the tail and the skin was bluntly detached from the subcutaneous fascia over a width of about 1 cm. At the laterally-exposed areas of each parabiont a 1 cm long incision of the peritoneum was made and the corresponding edges were sutured together joining the two peritoneal cavities. Finally the parabionts were joined by suturing the corresponding scapulas and the skin with Ethylon 5-0 (Ethicon, Albuquerque, NM, USA). Both parabionts were injected in parallel with 400 μl sRBC or saline as control. *Hemolytic anemia model involving PHZ*: C57BL/6J WT mice were administered 2 mg/mouse phenylhydrazine (PHZ; from Sigma-Aldrich, St. Louis, MO, USA) dissolved in 200 μL PBS i.p. Three days after injection, peripheral blood was drawn from the cheek and measured for RBC content on VetScan hematology analyzer (Abaxis Veterinary Diagnostics, Union City, CA, USA). Liver was excised after vascular perfusion with 20 ml sterile PBS, minced, and strained through a 40 μm-nylon mesh (BD Bioscience, San Jose, CA, USA). The single cell suspension was then stained with antibodies for flow cytometric analysis. *Brucella abortus-induced anemia model*: To induce anemia, animals were injected i.p. with 1×10^{9} particles per mouse of a commercially heat-killed *B. abortus* preparation (strain 1119-3; US Department of Agriculture, Animal and Plant Health Inspection Service, National Veterinary Services Laboratories, San Francisco, CA, USA). Control mice were injected i.p. with normal saline. During the experiments, mice were studied on days 0, 2, and 9 after injection. *Sickle cell anemia model:* Unless otherwise indicated, sickle cell disease

mice and transgenic controls were studied in steady-state. *Lineage Tracing Experiments: Radiation-free bone marrow chimeras.* 2 – 3 month old WT mice were treated with low dose busulfan (Busilvex: purchased from Pierre Fabre, Freiburg, Germany; 10 mg/kg, i.p.) and transplanted with 50 – 70 × 10^6 bone marrow cells obtained from GFP^+ mice 3 days later. Blood leukocyte chimerism (GFP positivity) was tested every week and reached typically 50 – 90% among Ly-$6C^{high}$ monocytes. 3 weeks after bone marrow transplantation, mice were treated with sRBC or PBS and sacrificed 4 – 7 days later and chimerism of organ-resident myelocytes was checked with flow cytometry with co-staining for lineage and myeloid cell markers. *tdTomato mice.* Pregnant *Cx3cr1-CreERT2* mice (mated with R26-tdT) were injected s.c. with tamoxifen (Sigma-Aldrich, 8 mg/animal in 400 μl corn oil) on days E13.5 and 15.5 to induce tdTomato expression in embryonic monocytes/macrophages. Pups were derived by Cesarian cut on day E21 and placed with nursing FVB/N dams. The *Cx3cr1-CreERT2*R26-tdT pups were distinguished from the genuine litter by coat color. At the age of 10 weeks (P70) mice were transplanted with GFP bone marrow after busulfan pre-conditioning (see *Radiation-free bone marrow chimeras*) and challenged with sRBC or PBS as described above (P91). Chimerism and tdTomato expression among blood leukocytes and organ-resident myelocytes was determined by flow cytometry. *FPN1-deficient rescue experiments:* $LysM^{Cre/+}$ $Slc40a1^{fl/fl}$ mice were treated with busulfan and transplanted with either $LysM^{+/+}$ $Slc40a1^{fl/fl}$ (WT) or $LysM^{Cre/+}$ $Slc40a1^{fl/fl}$ ($FPN1^{-/-}$) bone marrow cells as described above for WT mice. 3 weeks after transplantation mice were infused with sRBC and sacrificed 16 h later. Serum and organ samples were collected and processed for liver and kidney function parameters and histology.

Murine Cells

Collection: Peripheral blood was collected by retroorbital bleeding with heparinized capillaries and, where appropriate, erythrocytes were lysed in RBC Lysis buffer (Biolegend, San Diego, CA, USA). Spleen and liver were excised after vascular perfusion with 20 ml sterile PBS. Organs were minced and strained through a 40 μm-nylon mesh (BD Biosciences, San Jose, CA, USA). To increase the yield of hepatic macrophages, minced liver tissue was digested in 450 U/ml collagenase I, 60 U/ml DNase I and 60 U/ml hyaluronidase (Sigma-Aldrich, St. Louis, MO, USA) in PBS for 20 min at 37 °C while shaking. Cells were counted in a Neubauer chamber. *Sorting*: Murine monocytes, macrophages, neutrophils, B cells and T cells from blood, spleen and liver homogenates were isolated by FACS with a FACS Aria II cell sorter. For adoptive transfer and culture experiments murine spleen homogenates were enriched for monocytes prior to flow assisted cell sorting. In brief, splenocytes were incubated with 1 μl anti-CD11b (clone M1/70, BD Bioscience, San Jose, CA, USA) or anti-CD115 Ab (clone AFS98, ebioscience, San Diego, CA, USA) per 1 x 10^8 cells in sterile 2% FBS, 0.5% BSA in PBS for 30 min on ice, followed by MACS bead incubation and positive selection with a Midi MACS separator and LS column (all from Miltenyi, Bergisch Gladbach, Germany) according to the manufacturer's instruction. *Kupffer cells sorting in lineage tracing experiments*: To maximize the yield of Kupffer cells (KC), animals were perfused with Liberase™ (Roche, Mannheim, Germany) according to a published protocol[33]. The obtained single cell suspension was centrifuged at 30 g for 3 min to pellet hepatocytes, the supernatants centrifuged at 300 g for 5 min to pellet the non-parenchymal fraction. The pellets were

stained for Lineage (CD3, CD19, Ly-6G, NK1.1), CD45, CD11b and F4/80 markers. In case of marrow-transplanted WT mice, GFP^+ and GFP^- KC were sorted from PBS- and sRBC-transfused mice. In case of *Cx3cr1-CreERT2*R26-tdT mice infused with sRBC, $tdTomato^+$ GFP^- (eKC) and tdTomato- GFP^+ (mKC) Kupffer cells were sorted into cooled 0.5 ml Eppendorf tubes containing 350 μl RLT Buffer (Qiagen, Hilden, Germany) with addition of 1:100 β-mercaptoethanol. The amount of the sorted eKC and mKC was 5×10^4 cells per tube, at least 3 such tubes were collected per animal and pooled in the course of RNA isolation.

Human Cells

Collection: 5 persons (1 female, 4 males) undergoing cardiac surgery with the necessity for extracorporal circulation in the form of cardiopulmonary bypass (CPB) involving the Cell Saver® autologous blood recovery system (Haemonetics Corporation, Braintree, MA, USA) were enrolled in an observational study approved by Partners Human Research Committee (Protocol No. 2013P002596/MGH). Written informed consent was obtained in accordance with the Declaration of Helsinki from these persons. Indications for cardiac surgery were aortic valve replacement (n = 3), aortic valve replacement and concurrent coronary artery bypass grafting (n = 1) and repair of an aneurysm of the aortic sinus (n = 1). A mean volume of 755 ml of cell saver including autologous RBC but no packed RBC were transfused in the course of surgeries which had a mean duration of 242 min and a mean CBP time of 105 min. Peripheral blood samples were taken prior to, 15 min after, and 4 h after extracorporal circulation. *Sorting*: Human monocytes were isolated by FACS with a FACS Aria II cell sorter (BD Biosciences). Human peripheral blood mononuclear cells (hPBMC) were enriched for monocytes prior to FACS. PBMC were isolated from heparinized whole blood by the use of Ficoll density gradient centrifugation. For further enrichment hPBMC were incubated with 2 μl anti-HLA-DR (clone L243, BD Biosciences) or 2 μl anti-CD14 (clone MP9, BD Biosciences) per 1×10^8 cells in sterile 2% FBS, 0.5% BSA in PBS for 30 min on ice, followed by MACS bead incubation and positive selection with a Midi MACS separator and LS column according to the manufacturer's instruction.

Flow Cytometry

Cell suspensions were stained in PBS supplemented with sterile 2% FBS and 0.5% BSA. The following monoclonal antibodies were used for murine flow cytometric analysis: anti-Ly-6C (clone AL-21, BD Biosciences, San Jose, CA, USA), anti-CD45.1 (clone A20, Biolegend, San Diego, CA, USA), anti-CD45.2 (clone 104, BD Biosciences), anti-CD3e (clone 145-2C11, ebioscience, San Diego, CA, USA), anti-CD90.2 (clone 53-2.1, BD Biosciences), anti-CD19 (clone 6D5, Biolegend), anti-B220 (clone RA3-6B2, BD Biosciences), anti-MHCII (clone AF6-120.1, BD Biosciences), anti-F4/80 (clone BM8, Biolegend), anti-CD49b (clone DX5, BD Biosciences), anti-NK1.1 (clone PK136, BD Biosciences), anti-Ly-6G (clone 1A8, BD Biosciences), anti-CD11b (clone M1/70, BD Biosciences), anti-CD11c (clone HL3, BD Biosciences), anti-Ter119 (clone Ter-119, BD Biosciences), anti-CD115 (clone AFS98, ebioscience), anti-mMer (MerTK, clone 108928, R&D), anti-mFcgammRI (clone 290322, R&D), anti-CD14 (Sa14-2, Biolegend), anti-CD36 (HM36, Biolegend), anti-CD80 (16-10A1, Biolegend), anti-CD86 (GL-1, Biolegend), anti-CD206 (C068C2, Biolegend), anti-CD209a (MMD3, Biolegend), anti-CD278 (7E.17G9),

anti-MARCO (MCA 1849 FT, Biorad), anti-Tim-4 (RMT 4-54, eBioscience). Monoclonal rat-anti-mouse Ferroportin-1 (FPN1; Amgen, clone 1E11) antibody[34] was conjugated with a Pacific blue dye using the APEX™ Pacific Blue Antibody Labeling Kit (Life Technologies, Carlsbad, CA, USA) according to the manufacturer's instructions and compared against an isotype control mIgG2a PacBlue (clone MOPC-173, Biolegend). Specifically, erythrocytes were defined as $CD45^{-}$ $Ter119^{+}$. Monocytes were identified as $CD45^{+}$, Lin^{-} (Lin = CD3, CD90.2, CD19, B220, NK1.1, CD49b, Ly-6G), $CD11b^{+}$, $F4/80^{low}$, $MHCII^{low}$, $CD11c^{low}$, $CD115^{+}$ cells, subdivided into Ly-$6C^{high}$ and Ly-$6C^{low}$ populations. Neutrophils were identified as $CD45^{+}$, Lin^{+}, $CD11b^{+}$, $F4/80^{-}$, $MHCII^{low}$, $CD11c^{low}$, SSC^{high}, Ly-$6C^{int}$ cells. Red pulp macrophages (RPM) were identified as $CD45^{+}$, Lin^{-}, $CD11b^{low}$, $F4/80^{high}$ and KC as $CD45^{+}$, Lin^{-}, $CD11b^{int}$, $F4/80^{high}$ cells. The following antibodies were used for human flow cytometric analyses: anti-CD11b (clone ICRF44, BD Biosciences), anti-HLA-DR (clone L243, BD Bioscience), anti-CD16 (clone 3G8, BD Biosciences), anti-CD14 (clone MP9, BD Biosciences), anti-CD56 (clone NCAM16.2, BD Biosciences), anti-CD235a (clone GA-R2, BD Biosciences). Cells were first gated using FSC/SSC characteristics, and doublets were excluded by comparing FSC-height and -area signals. Classical monocytes were identified as HLA-DR^{+}, $CD11b^{+}$, $CD14^{high}$, $CD16^{-}$ and nonclassical monocytes as HLA-DR^{+}, $CD11b^{+}$, $CD14^{dim}$, $CD16^{+}$, $CD56^{-}$. Data were acquired on an LSRII (BD Biosciences) and analyzed with FlowJo v8.8.6 (Tree Star, Inc., Ashland, USA).

Cell and molecular biology

Cell culture: Human and murine monocyte subsets were cultured at 0.7×10^{6}/500 μl in RPMI-1640 supplemented with 10% FBS, 2 mM L- glutamine, 100 U/ml penicillin, 100 μg/ml streptomycin, in a 24 well plate (Falcon™; obtained from Fisher Scientific, Pittsburgh, PA, USA). Recombinant (r) Csf1/rCSF1 (50 ng/ml, Preprotech, Rocky Hill, NJ, USA), rCsf2/rCSF2 (100 ng/ml, Preprotech, Rocky Hill, NJ, USA) were added to the cell cultures for 72 h. 6 h before termination of the experiment a 10-fold excess of sRBC was added. *In vitro RBC uptake:* 50,000 murine FAC-sorted cells were seeded onto 24-well plates in 500 μl RPMI-1640 supplemented with 10% autologous serum, L-glutamine and antibiotics. Subsequently, cells were stimulated with PBS or 500,000 pkh26-labeled naive yRBC or sRBC for 1 h. Cells were washed 2× in 1× RBC lysis buffer to remove surplus RBC, and incubated in RPMI-1640 for another 2 h. Thereafter, cells were washed twice with 1 ml of 1× RBC lysis buffer for 10 min before antibody staining for flow cytometry. To test for a possible cell-cell transfer of pkh26, 50,000 FAC-sorted cells per population tested were seeded in mono-culture or co-culture in 24-well plates for up to 72 h. To identify individual populations after co-culture, KC were harvested from $CD45.2^{+}$ GFP^{+} donors whereas tMΦ and monocytes were of the $CD45.1^{+}$ genotype (and thus GFP^{-}). To identify the cellular source of Ccl2, Ccl3 and Csf1, individual cell populations were FAC-sorted from liberase-perfused livers of mice under steady state conditions (KC) or 16 h after elicitation of tMΦ and monocytes with sRBC. 250,000 cells were seeded onto 6-well plates in 1 ml RPMI-1640 supplemented with 10% FBS, L-glutamine and antibiotics. After additional 16 h of culture, supernatants were frozen to measure chemokine/growth factor concentrations by means of a specific ELISA strictly according to the manufacturer's (R&D) protocol. *^{59}Fe–release assay:* The iron release assay was performed with the use of ^{59}Fe-citrate (Perkin Elmer, Llantrisant, UK). Sorted KC and RPM were seeded in 24 well plates, each well with

30,000 cells. The release assay was performed exactly as described previously[2]. In brief, seeded KC/RPM were washed three times with 1 ml of serum-free, HEPES-buffered DMEM (2 mM L-glutamine, 50 mg/ml ampicillin, 25 mM HEPES (Sigma-Aldrich), pH 7.4) and incubated in 2 ml of this solution. Thereafter 5 μM ^{59}Fe-citrate was added to the samples and incubated for 2 h to allow iron loading. Cells were then washed with 500 μL of serum-free, HEPES-buffered DMEM and incubated for 2 h. Following three washing cycles with 500 μL of 0.9% NaCl plus 50 μM $^{58}FeCl_3$, cells were lysed with 400 μl 0.1% SDS and quantified by a γ-Counter. Protein concentration was determined by BCA assay (BCA Protein Assay Kit; Pierce Thermo Scientific). *Western blotting*: Cytosolic protein was extracted from freshly isolated tissue and Western blotting was performed as previously described[35]. Anti-Ferritin antibody (2 μg/ml, Dako, Austria), rabbit anti-rat-Ferroportin-antibody[2], rabbit anti-mouse-Hmox1 antibody (ADI-SPA-895-D, Enzo Life Sciences, 1:1000), rabbit anti-mouse/human-TfR1 (H68.4, Invitrogen, 1:1000) or anti-actin (2 μg/ml, Sigma, Germany) were used as described previously. NIH ImageJ was used to quantify Western blot bands densitometrically. *ELISA:* Cytosolic protein was isolated from liver and spleen by 10 consecutive freeze-thaw cycles performed in PBS in the presence of 1× Halt™ Protease inhibitor cocktail (Pierce Pierce Thermo Scientific, Grand Island, NY, USA). Homogenous extracts were centrifuged at 10,000 g for 10 min and supernatants used as input in specific ELISA kits (LifeSpan BioSciences, Seattle, WA, USA). *RNA preparation from tissue, reverse transcription, and real-time PCR:* Total RNA preparation from nitrogen-frozen mouse tissue and cultured cells, reverse transcription, and real-time polymerase chain reaction (RT-PCR) were performed as previously described[33]. For total RNA preparation from 3×10^4 freshly sorted human and murine monocytes, cells were lysed in RLT buffer with 1% β-mercaptoethanol. RNA was isolated with the RNeasy Micro Kit (Qiagen, Venlo, Netherlands) followed by cDNA transcription.

Primer sets without probes used SYBR Green detection. They were designed by Primer3 software or the NCBI Primer Blast. The following primers and probes were used:

Hamp (hepcidin): fw 5′-GGC AGA CAT TGC GAT ACC AAT-3′, rv 5′-TGC AAC AGA TAC CAC ACT GGG AA-3′, probe FAM-CCA ACT TCC CCA TCT GCA TCT TCT GC-BHQ1.

Slc40a1: fw 5′-CTA CCA TTA GAA GGA TTG ACC AGC T-3′, rv 5′-CAA ATG TCA TAA TCT GGC CGA-3′, probe FAM-CAA CAT CCT GGC CCC CAT GGC-BHQ1.

SLC40A1: fw 5′-TGA CCA GGG CGG GAG A -3′, rv 5′-GAG GTC AGG TAG TCG GCC AA-3′, probe FAM-CAC AAC CGC CAG AGA GGA TGC TGT G-BHQ1.

Ccl2: fw 5′-CTT CTG GGC CTG CTG TTC A-3′, rv 5′-CCA GCC TAC TCA TTG GGA TCA-3′, probe FAM-CTC AGC CAG ATG CAG TTA ACG CCC C-BHQ1.

Ccl3: fw 5′-AGC TGA CAC CCC GAC TGC′, rv 5′-GTC AAC GAT GAA TTG GCG TG-3′, probe FAM-TGC TGC TTC TCC TAC AGC CGG AAG AT-BHQ1.

Ccl5: fw 5′-GGA GTA TTT CTA CAC CAG CAG CAA -3′, rv 5′-CAC ACA CTT GGC GGT TCC TT-3′, probe FAM-TGC AGT CGT GTT TGT C -BHQ1

Slc11a2: fw 5′-GGA CTG TGG ACG CTC GGT AA -3′, rv 5′-AAT GTT GCC ACC GCT GGT -3′, probe: FAM-CAT CTC GAA AGT CCT GCT GAG CGA AGA-BHQ1

Tgf1: fw 5′-ACT GGA GTT GTA CGG CAG TGG -3′, rv 5′-TGC AGT GAG CGC TGG ATC GA -3′, probe: FAM-TGA ACC AAG GAG ACG GAA TAC AGG GCT-BHQ1

Il6: fw 5′-TGT TCT CTG GGA AAT CGT GGA -3′, rv 5′-AAG TGC ATC ATC GTT GTT CAT ACA-3′, probe: FAM-ATG AGA AAA GAG TTG TGC AAT GGC AAT TCT-BHQ1

Il10: fw 5′-CCA GAG CCA CAT GCT CCT AGA -3′, rv 5′-TGG TCC TTT GTT TGA AAG AAA GTC T -3′, probe: FAM-TGC GGA CTG CCT TCA GCC AGG-BHQ1

Tfrc: fw 5′-CGC TTT GGG TGC TGG TG -3′, rv 5′-GGG CAA GTT TCA ACA GAA GAC C -3′, probe: FAM-CCC ACA CTG GAC TTC GCC GCA-BHQ1

Hmox1: fw 5′-CGA CAG CAT GCC CCA GGA TTT GTC -3′, rv 5′-GTG ATG GAG CGT CCA CAG C -3′, probe: FAM-TGG TGG CCT CCT TCA AGG-BHQ1

Il1b: fw 5′-ACC TGT CCT GTG TAA TGA AAG ACG -3′, rv 5′-TGG GTA TTG CTT GGG ATC CA -3′, probe: FAM-CAC ACC CAC CCT GCA GCT GGA GA-BHQ1

Csf1: fw 5′-CCC AGA TCC CTG AGT C-3′, rv 5′-GTC TCG ATG GCT CCT C-3′

Nfe2l2: fw 5′-AGT CCC AGC AGG ACA T- 3′, rv 5′-AGT CAA ACA CTT CTC GAC TT- 3′

NFE2L2: fw 5′-TTG TAG ATG ACA ATG AGT CAC-3′, rv 5′-GAC TGA GCC TGA TTA GTA GC-3′

Cx3cl1: fw 5′-TGC TGC TTC TCC TAC AGC CGG AAG AT-3′, rv 5′-TGC TGC TTC TCC TAC AGC CGG AAG AT-3′

Cxcl12: fw 5′-TGC TGC TTC TCC TAC AGC CGG AAG AT-3′, rv 5′-TGC TGC TTC TCC TAC AGC CGG AAG AT-3′

Ccl21: fw 5′-TGC TGC TTC TCC TAC AGC CGG AAG AT-3′, rv 5′-TGC TGC TTC TCC TAC AGC CGG AAG AT-3′

Cyp2e1: fw 5′-GAG GTG CTA CTG AAC CAC AAG- 3′, rv 5′-ACG GAG GAT ACT TAG GGA AAA CC-3′

Fas: fw 5′-AGG TGG TGA TAG CCG GTA TGT-3′, rv 5′-TGG GTA ATC CAT AGA GCC CAG-3′

Srebf1: fw 5′-CCG GGG AAC TTT TCC TTA AC-3′, rv 5′-TGG TTG TTG ATG AGC TGG AG-3′

Ppara: fw 5′-CTG TCA TCA CAG ACA CCC TCT C-3′, rv 5′-TAT TCG ACA CTC GAT GTT CAG G-3′

Cd163: fw 5′-CAT GTG GGT AGA TCG TGT GC -3′, rv 5′-TGT ATG CCC TTC CTG GAG TC -3′

Retnla: fw 5′-CAT GTG GGT AGA TCG TGT GC -3′, rv 5′-CAG TAG CAG TCA TCC CAG CA -3′

Chi3l3: fw 5′-CCA GCA GAA GCT CTC CAG AA -3′, rv 5′-GTA CAC AGG CAG GGG TCA AT -3′

Mrc1: fw 5′-ATG CCA AGT GGG AAA ATC TG -3′, rv 5′-TGT AGC AGT GGC CTG CAT AG -3′

Spic: fw 5′-CCA CTT GGT TTT CCT GAA CGT -3′, rv 5′-TTG CGG AAA TGT CAG CGA GTA -3′

Pu1: fw 5′-TGG AGA AGC TGA TGG CTT GG -3′, rv 5′-CCA GCA GGA ACT GGT ACA GG -3′

Irf4: fw 5′-AAT CCC CAT TGA GCC AAG CA -3′, rv 5′-CTC GTC GTG GTC AGC TCT TT -3′

Irf5: fw 5′-ACC TGT CCT GTG TAA TGA AAG ACG -3′, rv 5′-TGG AAG TCA CGG CTT TTG TTA AG -3′

Clec4f: fw 5′-TTT TGT GGT GGC TTC ACA GC -3′, rv 5′-TCC AGA GTT GTT GCT TCC CC -3′

Bach1: fw 5′-GTC TCG GCT CCG GTC G -3′, rv 5′-TCG TAG GCA AAT ACC GC ACT -3′

Melting curve analysis was performed with each run to test specificity in Sybr green assays. Agarose gel electrophoresis of PCR products was performed with first primer tests to ensure a single product. RT-PCR was performed on a Bio-Rad CFX96 light cycler. Ssofast Probes Supermix and Ssofast EvaGreen Supermix (Bio-Rad, Vienna, Austria) were used according to the manufacturer's instructions. Relative quantities were calculated by Bio-Rad's CFX Manager software based on a standard curve calculated from four serial 10-fold dilutions of the standard. A standard curve was pipetted on each individual plate.

Chemistry

Blood samples from anesthetized mice were collected. Whole blood was further processed by centrifugation at 10,000 rpm for 5 min for serum isolation, which was then tested using comprehensive metabolic panels (AST, ALT, BUN, Amylase) and an Abaxis Piccolo chemistry analyzer.

Histology & Microscopy

Immunofluorescence: Cell specific uptake of pkh26-labeled RBC was visualized by immunofluorescence microscopy. Sorted WBC populations from liver, spleen, and blood were prepared to a cell suspension of 2.5×10^5 cells/ml. 200 µl of suspension per cuvette were centrifuged at 500 rpm for 3 min. After air drying cells were embedded in Vectashield Mounting Medium with DAPI H1200 (Vector Lab, Burlingame, CA) and analyzed using a Nikon 80i upright epifluorescence microscope with Hamamatsu Orca CCD camera and complete image analysis software (IP Lab). *Transmission Electron Microscopy*: Tissues were fixed in 2% glutaraldehyde in 0.1 M sodium cacodylate buffer, pH 7.4 (Electron Microscopy Sciences, Hatfield, PA) overnight at 4 °C. The tissues were rinsed in buffer, post-fixed in 1% osmium tetroxide in cacodylate buffer for 1 h at RT, rinsed in buffer and dehydrated through a graded series of ethanol to 100%, followed by propylene oxide, 100%. They were then infiltrated with Epon resin (Ted Pella, Redding, CA) in a 1:1 solution of Epon:propylene oxide overnight on a rocker at RT. The following day they were placed in fresh Epon for several hours and then embedded in Epon overnight at 60 °C. Thin sections were cut on a Leica EM UC7 ultramicrotome, collected on formvar-coated grids, stained with uranyl acetate and lead citrate and examined in a JEOL JEM 1011 transmission electron microscope at 80 kV. Images were collected using an AMT digital imaging system (Advanced Microscopy Techniques, Danvers, MA).

Iron detection

Prussian blue staining: Liver tissue was embedded in Tissue-Tek O.C.T. compound (Sakura Finetek, Alphen aan den Rijn, Netherlands), frozen and sectioned into 6 µm slices. Kidney tissue was fixed overnight in 10% paraformaldehyde, and embedded in paraffin before sectioning. Iron staining Kit (Sigma, Saint Louise MO, USA) was used for Prussian blue staining according to manufacturer's instructions. Tissues were stained by a histologist single-blinded to study design and treatment group. A Zeiss Axioscope 40 microscope with a 40× lens and an AxioCam MRc5 (Carl Zeiss AG, Oberkochen, Germany) was used. The slides were scanned by a digital scanner Nanozoomer 2.0RS (Hamamatsu, Japan). Representative fields were photodocumented using a pixellink® system. *Serum and Tissue Iron measurement*: Serum iron concentrations were measured with a commercially available colorimetric iron quantification kit (QuantiChrom™ Iron Assay Kit, BioAssay Systems, Hayward, CA, USA). Tissue iron was measured with a colorimetric method as previously described[36] adapted to a 96-well format as detailed elsewhere[37]. Briefly, 20–30 mg tissues were homogenized in cytoplasmic lysis puffer (25 mM Tris-HCl, pH 7.4, 40 mM KCl, 1% Triton X-100) supplemented with 1 µg/ml aprotinin and 1 µg/ml leupeptin (all from Sigma, St Louis, MO, USA) and centrifuged at 20,000 g for 15 min. 100 µl of the obtained supernatant was supplemented with 50 µl acid hydrolysate solution (7 ml HCl 37%, 3 g TCA diluted with aqua destillata (a.d.) to 10 ml). The samples were incubated at 65 °C with vertical mixing (100 rpm) for 24 h. Samples were then centrifuged at 3,000 g for 15 min. 60 µl of the obtained supernatant from each sample were transfered into a 96 well plate in doublets and 160 µl of a colorimetric solution (1:1 mixture of 15.6 g sodium acetate diluted to 45 mL with a.d., and 17 mg of bathophenanthroline disulfonic acid and 22 mg L-ascorbic acid diluted to 5 mL with a.d.) was added to each sample and a Fe^{2+} standard curve was prepared via serial dilution of a purchased 10 mg/dL $FeSO_4$ stock (BioAssay Systems®,

Hayward, CA, USA). Probes were incubated for 15 min at RT to allow colorimetric reaction, following photometric measurement of optical density at 539 nm. The calculated iron quantity was normalized against the wet tissue weight for each sample. *Intracellular iron determination by graphite furnace atomic absorption spectrometry in sorted cells:* A Detection was carried out in a single-blinded manner by utilizing a PerkinElmer Analyst 800 equipped with a transversely heated graphite atomizer (THGA). A Zeeman-effect background correction was realized by a 0.8 T magnetic field, oriented longitudinally with respect to the optical path. A PerkinElmer Lumina single element iron hollow cathode lamp was driven at a constant current of 30 mA after proper equilibration (i.e. ≥ 20 min). For the absorption measurements, the 248.3 nm line (spectral bandwidth 0.7 nm) was chosen. The samples were suspended in 200 µl of a 0.1 % (v/v) solution of nitric acid (Rotipuran Supra, 69 %, Carl Roth GmbH, Karlsruhe, Germany) in high-purity water (Milli-Q, Merck-Millipore, Darmstadt, Germany) by extended periods (i.e. ≥ 30 min) of vortexing and ultrasonication at 30–40 kHz. After an initial estimation of the samples' iron quantity, a five-point linear calibration was established in the range between 0 (i.e. < 0.004 µM) and 0.106 µM. The calibration standards were prepared by diluting a 0.1 M standard stock solution of $(NH_4)_2Fe(SO_4)_2$ (Merck-Millipore, Darmstadt, Germany) with a 0.1 % (v/v) aqueous solution of nitric acid (vide supra). The absence of detectable iron (i.e. < 0.004 µM) in the dilution agent as well as in the sample cups and the glassware was verified throughout the analyses. A linear fit of the 15 data points (k = 0.978, d = 0.006 µM) yielded a coefficient of determination of 0.992. Samples with iron concentrations exceeding the calibration range (i.e. ≥ 0.106 µM) were diluted appropriately. The blank solution, the calibration standards and the samples were supplied to the atomizer in randomized fashion as triplicates, utilizing a PerkinElmer AS-800 autosampler with an injection volume of 20 µl. The solvent was evaporated by a slow temperature gradient to 130 °C, ashing took place at a maximum temperature of 1000 °C and the atomization profile was read at 2000 °C. The graphite tube, being protected against oxidation by high-purity argon (99.999 %, Messer Austria GmbH, Gumpoldskirchen, Austria) was cleaned-out after each analysis at 2450 °C. The integrity of each analysis was verified by a visual inspection of the respective time-dependent atomization profile. *Enhanced labile plasma iron detection*. eLPI (enhanced labile plasma iron) was assessed by the FeROS eLPI kits, a fluorescence-based assay intended for *in vitro* semiquantitative detection of both over and cryptic redox active forms of NTBI (Aferrix Tel Aviv, Israel). eLPI > 0.3 units indicated the potential for iron-mediated production of reactive oxygen species in the sample.

Microarray measurement and microarray data processing

Total RNA was isolated from the eKC and mKC sorted from *Cx3cr1-CreERT2*R26-tdT mice with the RNeasy Micro Kit (Qiagen, Hilden, Germany) according to manufacturer's protocol. Quality and quantity of RNA was estimated with Bioanalyzer with Nano total RNA Chips (Agilent, Santa Clara, CA, USA), the RIN values exceeded 7.8 for all samples used for microarray measurement. Total RNA was amplified, fragmented and labeled with biotin using the GeneChip WT Pico Reagent Kit (Affymetrix, Santa Clara, CA, USA) and samples were hybridized to GeneChip Mouse ST Arrays 2.0 according to the manufacturer's instructions. Probeset signal intensities were background-corrected and normalized using the RMA algorithm. Significantly regulated genes were identified using paired-T tests (pairing

by animal, limma package of R/Bioconductor) with Benjamini-Hochberg correction for multiple testing. Genes regulated at least 1.5 fold with $p < 0.1$ were considered significant. The microarray analysis was done with CARMAweb 1.5 software[38].

Statistics

Results are expressed as Means ± SEM or ± SD as indicated. Where appropriate, the sample size required to reach statistical power was calculated assuming an alpha = 0.05 (P-value) and a beta = 0.1 (90%). Statistical tests included the Kolmogorov-Smirnov test or D'Agostino & Pearson omnibus normality test (depending on sample number) used to test for normality distribution. F-Test was used to compare variances. If variances were significantly different specific corrections were used as stated in detail in each figure legend. Calculations for statistical differences between various groups were carried out by ANOVA technique and Bonferroni or Dunnett correction for multiple tests. Otherwise 2-tailed unpaired Student's t test was used. In case of non-normality in distribution a Mann-Whitney U test was used. For serial comparisons in human subjects, the 2-tailed paired Student's t test was used. Calculations for statistical differences between various groups were carried out by Kruskal-Wallis Dunn's Multiple Comparison Test. $P < 0.05$ was used to determine statistical significance of parametric and non parametric data. Gene expression data clustering (average linkage algorithm, Euclidean distance measure) and heat map representation were done with the Genesis software[39].

Supplementary Material

Refer to Web version on PubMed Central for supplementary material.

Acknowledgments

This work was supported in part by NIH grants 1R01HL095612, R01HL128264, R56AI104695 and the Massachusetts General Hospital's Howard M. Goodman Fellowship (to F.K.S.) and R01DK071837 (to H.Y.L). I. T. was supported by the Max Kade Foundation and grants by the Austrian Science Fund (FWF) (P28302-B30 and P24749-B13)). I.H. (HI 1573/1-1, HI 1573/2-1) and G. F. W. were supported by the German Research Foundation. M. Nairz was supported by an FWF Erwin Schroedinger Fellowship (J3486-B13). L. M. S. G. and N.K.H. was supported by the Boehringer Ingelheim Fonds. F. W. was supported by the National Natural Science Foundation of China (31530034 and 31225013). We thank D. Capen with help in electron microscopy, N. Bonheur and M. Waring for help with cell sorting, A. Lindau for technical assistance, C. Haerdtner, J. Kornemann, J. Zou for help with flow cytometry, D. Brown for interpretation of electron microscopy images, C. Robbins for the mouse drawing, and K. Joyes for editing the manuscript.

References for main text

1. Hentze MW, Muckenthaler MU, Galy B, Camaschella C. Two to tango: regulation of Mammalian iron metabolism. Cell. 2010; 142:24–38. [PubMed: 20603012]
2. Theurl I, et al. Regulation of iron homeostasis in anemia of chronic disease and iron deficiency anemia: diagnostic and therapeutic implications. Blood. 2009; 113:5277–5286. [PubMed: 19293425]
3. Weinberg ED. The hazards of iron loading. Metallomics. 2010; 2:732–740. [PubMed: 21072364]
4. Ganz T. Macrophages and systemic iron homeostasis. J Innate Immun. 2012; 4:446–453. [PubMed: 22441209]
5. Higgins JM, Mahadevan L. Physiological and pathological population dynamics of circulating human red blood cells. Proc Natl Acad Sci U S A. 2010; 107:20587–20592. [PubMed: 21059904]

6. Weiss G, Goodnough LT. Anemia of chronic disease. N Engl J Med. 2005; 352:1011–1023. [PubMed: 15758012]
7. Luten M, et al. Survival of red blood cells after transfusion: a comparison between red cells concentrates of different storage periods. Transfusion. 2008; 48:1478–1485. [PubMed: 18482180]
8. Prasad AS, et al. Hereditary sideroblastic anemia and glucose-6-phosphate dehydrogenase deficiency in a Negro family. J Clin Invest. 1968; 47:1415–1424. [PubMed: 4871209]
9. Tinmouth A, Fergusson D, Yee IC, Hebert PC. Clinical consequences of red cell storage in the critically ill. Transfusion. 2006; 46:2014–2027. [PubMed: 17076859]
10. Wilairat P, Kittikalayawong A, Chaicharoen S. The thalassemic red cell membrane. Southeast Asian J Trop Med Public Health. 1992; 23(Suppl 2):74–78. [PubMed: 1298998]
11. Knutson MD, Oukka M, Koss LM, Aydemir F, Wessling-Resnick M. Iron release from macrophages after erythrophagocytosis is up-regulated by ferroportin 1 overexpression and down-regulated by hepcidin. Proc Natl Acad Sci U S A. 2005; 102:1324–1328. [PubMed: 15665091]
12. Soares MP, Hamza I. Macrophages and Iron Metabolism. Immunity. 2016; 44:492–504. [PubMed: 26982356]
13. Hod EA, et al. Transfusion of red blood cells after prolonged storage produces harmful effects that are mediated by iron and inflammation. Blood. 2010; 115:4284–4292. [PubMed: 20299509]
14. Zocchi E, et al. Hepatic or splenic targeting of carrier erythrocytes: a murine model. Biotechnol Appl Biochem. 1987; 9:423–434. [PubMed: 3675876]
15. Terpstra V, van Berkel TJ. Scavenger receptors on liver Kupffer cells mediate the in vivo uptake of oxidatively damaged red blood cells in mice. Blood. 2000; 95:2157–2163. [PubMed: 10706889]
16. Nemeth E, et al. Hepcidin regulates cellular iron efflux by binding to ferroportin and inducing its internalization. Science. 2004; 306:2090–2093. [PubMed: 15514116]
17. Haldar M, et al. Heme-mediated SPI-C induction promotes monocyte differentiation into iron-recycling macrophages. Cell. 2014; 156:1223–1234. [PubMed: 24630724]
18. Kohyama M, et al. Role for Spi-C in the development of red pulp macrophages and splenic iron homeostasis. Nature. 2009; 457:318–321. [PubMed: 19037245]
19. Gardenghi S, et al. Distinct roles for hepcidin and interleukin-6 in the recovery from anemia in mice injected with heat-killed Brucella abortus. Blood. 2014; 123:1137–1145. [PubMed: 24357729]
20. Sasu BJ, et al. Antihepcidin antibody treatment modulates iron metabolism and is effective in a mouse model of inflammation-induced anemia. Blood. 2010; 115:3616–3624. [PubMed: 20053755]
21. Ryan TM, Ciavatta DJ, Townes TM. Knockout-transgenic mouse model of sickle cell disease. Science. 1997; 278:873–876. [PubMed: 9346487]
22. Gautier EL, et al. Gene-expression profiles and transcriptional regulatory pathways that underlie the identity and diversity of mouse tissue macrophages. Nat Immunol. 2012; 13:1118–1128. [PubMed: 23023392]
23. Robbins CS, et al. Local proliferation dominates lesional macrophage accumulation in atherosclerosis. Nat Med. 2013; 19:1166–1172. [PubMed: 23933982]
24. Goldmann T, et al. A new type of microglia gene targeting shows TAK1 to be pivotal in CNS autoimmune inflammation. Nat Neurosci. 2013; 16:1618–1626. [PubMed: 24077561]
25. Yona S, et al. Fate mapping reveals origins and dynamics of monocytes and tissue macrophages under homeostasis. Immunity. 2013; 38:79–91. [PubMed: 23273845]
26. Geissmann F, et al. Development of monocytes, macrophages, and dendritic cells. Science. 2010; 327:656–661. [PubMed: 20133564]
27. Sarrazin S, Sieweke M. Integration of cytokine and transcription factor signals in hematopoietic stem cell commitment. Semin Immunol. 2011; 23:326–334. [PubMed: 21937237]
28. Marro S, et al. Heme controls ferroportin1 (FPN1) transcription involving Bach1, Nrf2 and a MARE/ARE sequence motif at position -7007 of the FPN1 promoter. Haematologica. 2010; 95:1261–1268. [PubMed: 20179090]

29. Nairz M, et al. Nitric oxide-mediated regulation of ferroportin-1 controls macrophage iron homeostasis and immune function in Salmonella infection. J Exp Med. 2013; 210:855–873. [PubMed: 23630227]
30. Kovtunovych G, Eckhaus MA, Ghosh MC, Ollivierre-Wilson H, Rouault TA. Dysfunction of the heme recycling system in heme oxygenase 1-deficient mice: effects on macrophage viability and tissue iron distribution. Blood. 2010; 116:6054–6062. [PubMed: 20844238]
31. Zhang Z, et al. Ferroportin1 deficiency in mouse macrophages impairs iron homeostasis and inflammatory responses. Blood. 2011; 118:1912–1922. [PubMed: 21705499]
32. Swirski FK, et al. Identification of splenic reservoir monocytes and their deployment to inflammatory sites. Science. 2009; 325:612–616. [PubMed: 19644120]
33. Theurl M, et al. Kupffer cells modulate iron homeostasis in mice via regulation of hepcidin expression. J Mol Med (Berl). 2008; 86:825–835. [PubMed: 18521557]
34. Ross SL, et al. Molecular mechanism of hepcidin-mediated ferroportin internalization requires ferroportin lysines, not tyrosines or JAK-STAT. Cell Metab. 2012; 15:905–917. [PubMed: 22682226]
35. Ludwiczek S, et al. Ca2+ channel blockers reverse iron overload by a new mechanism via divalent metal transporter-1. Nat Med. 2007; 13:448–454. [PubMed: 17293870]
36. Torrance JD, Bothwell TH. A simple technique for measuring storage iron concentrations in formalinised liver samples. S Afr J Med Sci. 1968; 33:9–11. [PubMed: 5676884]
37. Grundy MA, Gorman N, Sinclair PR, Chorney MJ, Gerhard GS. High-throughput non-heme iron assay for animal tissues. J Biochem Biophys Methods. 2004; 59:195–200. [PubMed: 15163531]
38. Rainer J, Sanchez-Cabo F, Stocker G, Sturn A, Trajanoski Z. CARMAweb: comprehensive R- and bioconductor-based web service for microarray data analysis. Nucleic Acids Res. 2006; 34:W498–503. [PubMed: 16845058]
39. Sturn A, Quackenbush J, Trajanoski Z. Genesis: cluster analysis of microarray data. Bioinformatics. 2002; 18:207–208. [PubMed: 11836235]

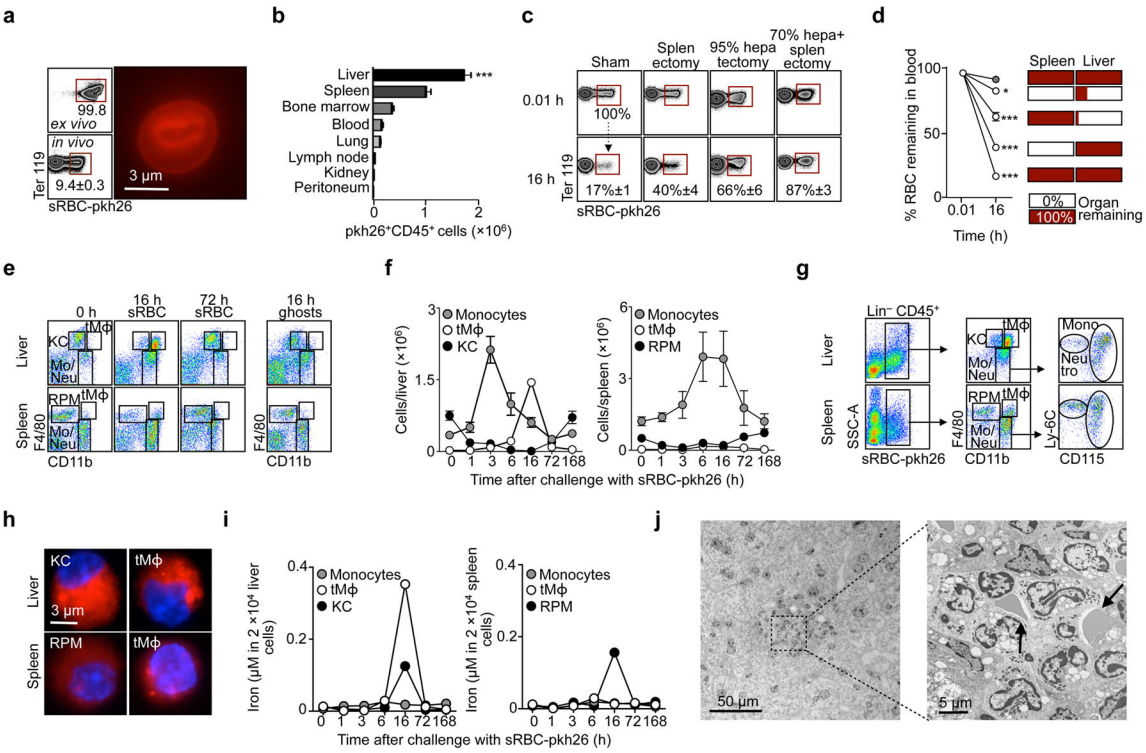

Figure 1. Myeloid cells in the liver are the major scavengers of stressed erythrocytes

(**a**) *Ex vivo* labeling of isolated erythrocytes (Ter119^{+}) and their identification (pkh26^{+}) amongst all erythrocytes 0.01 h after i.v. injection into congenic recipients. Means ± SEM; [n = 5 per group]. (**b**) Total number of CD45^{+} WBC that have ingested pkh26-labeled sRBC 16 h after delivery. Means ± SEM; [n = 5 per group, except peritoneum n = 3; *** P < 0.001 compared to each of the other organs; Anova and Dunnett's Multiple Comparison Test]. (**c**) Representative dot plots (1 of 3 experiments) and (**d**) quantification showing the effects of splenectomy, hepatectomy, and a combination thereof on the distribution of pkh26^{+} Ter119^{+} CD45^{-} cells in the circulation 0.01 h and 16 h after sRBC delivery. sRBC (white circles) or young RBC (yRBC, grey circles) were injected 1 d after surgery. Means ± SEM; [n = 4 for the yRBC, splenectomy and sham groups; n = 3 for hepatectomy and for hepatectomy combined with splenectomy; *P < 0.05, ***P < 0.001 compared to young RBC (yRBC); Anova and Dunnett's Multiple Comparison Test]. (**e**) Representative dot plots (1 of 3 experiments) showing gating for F4/80^{high} CD11b^{int} KC, F4/80^{low} CD11b^{high} monocytes (Mo)/neutrophils (Neu) and F4/80^{high} CD11b^{high} tMΦ in the liver and F4/80^{high} CD11b$^{int/low}$ RPM, F4/80^{low} CD11b^{high} Mo/Neu, and F4/80^{high} CD11b^{high} tMΦ in the spleen in steady state (0 h), 16 h, and 72 h after sRBC challenge. All cells gated as CD45^{+} Lin^{-} (CD3, CD19, NK1.1) leukocytes in liver and spleen 16 h after ghost challenge (on the right). (**f**) Dynamics of indicated leukocyte populations in liver (left) and spleen (right) after sRBC challenge. Means ± SD; [n = 6 for time-point 0, n = 3 for all other time-points]. (**g**) Representative dot plots (1 of 3 experiments) showing uptake of pkh26^{+} sRBC in liver and spleen by KC, RPM, tMΦ, and Mo/Neu 16 h after delivery. (**h**) Cytoplasmic pkh26 staining in KC, RPM, and tMΦ sorted from the liver and spleen 16 h after sRBC delivery. Blue denotes nuclei with DAPI staining and red denotes pkh26-sRBC. (**i**) Dynamics of iron

content measured by atomic absorption spectroscopy (AAS) in sorted leukocyte populations in liver (left) and spleen (right) after sRBC challenge (each sample pooled from 3–6 mice). (**j**) Transmission electron microscopy of a liver section, 16 h after sRBC challenge, showing peri-hepatocellular leukocyte infiltrate surrounding RBC (arrows).

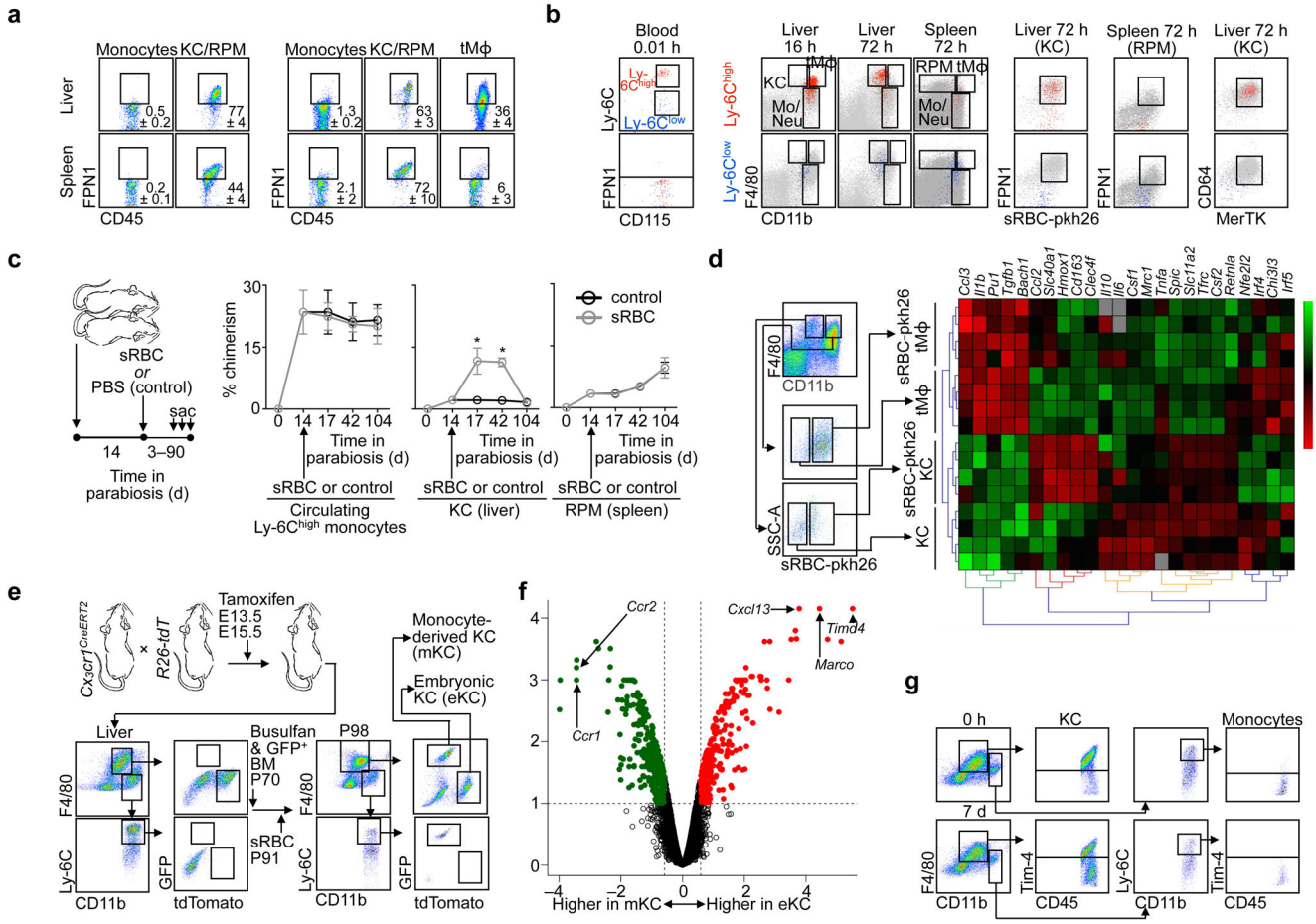

Figure 2. Ly-6C^{high} monocytes differentiate to FPN1^{+} macrophages for transient erythrocyte removal

(**a**) Representative dot plots (1 of 3 experiments) showing FPN1 expression in steady state (4 panels on the left) in different WBC populations of the liver and spleen and 16 h after sRBC challenge (6 panels on the right), Means ± SEM; [n = 5 per group]. (**b**) Representative dot plot (1 of 2 experiments) overlays showing adoptively transferred GFP^{+} Ly-6C^{high} (red) and Ly-6C^{low} (blue) monocytes differentiating in the liver and spleen at 16 h and 72 h after sRBC challenge. Gray dots represent endogenous populations in the overlay. An overlay of monocytes in the blood 0.01 h after transfer is shown on the left. (**c**) Parabiosis experiment outline and graphs showing time course of chimerism for circulating monocytes, KC, and RPM in steady state (control) and after sRBC challenge. Means ± SEM; [n = 4 per group and time point; * $P < 0.05$; Mann-Whitney test]). (**d**) Iron and immune-specific gene expression in sRBC-loaded and unloaded KC and liver tMΦ 16 h after sRBC challenge. Representative dot plots on the left show gating strategy for cell isolation. Green = low expression. Red = high expression. (**e**) Scheme and data of formal lineage tracing experiments involving Cx3cr1-CreERT2 females crossed with R26-tdT males. (**f**) Whole-genome expression profiling in mKC and eKC [n = 3 per group]. Volcano plot depicts -log$_{10}$ Benjamini-Hochberg-corrected p-value versus log$_2$ fold-regulation for each gene. Genes significantly augmented ($p_{Benjamini\text{-}Hochberg} < 0.1$ and fold regulation > 1.5) in mKC and

eKC are highlighted in green and red, respectively. (**g**) Tim-4 cell surface expression in liver KC and monocytes in steady state (0 h) and 7 d after sRBC challenge. Representative dot plots (1 of 3 experiments).

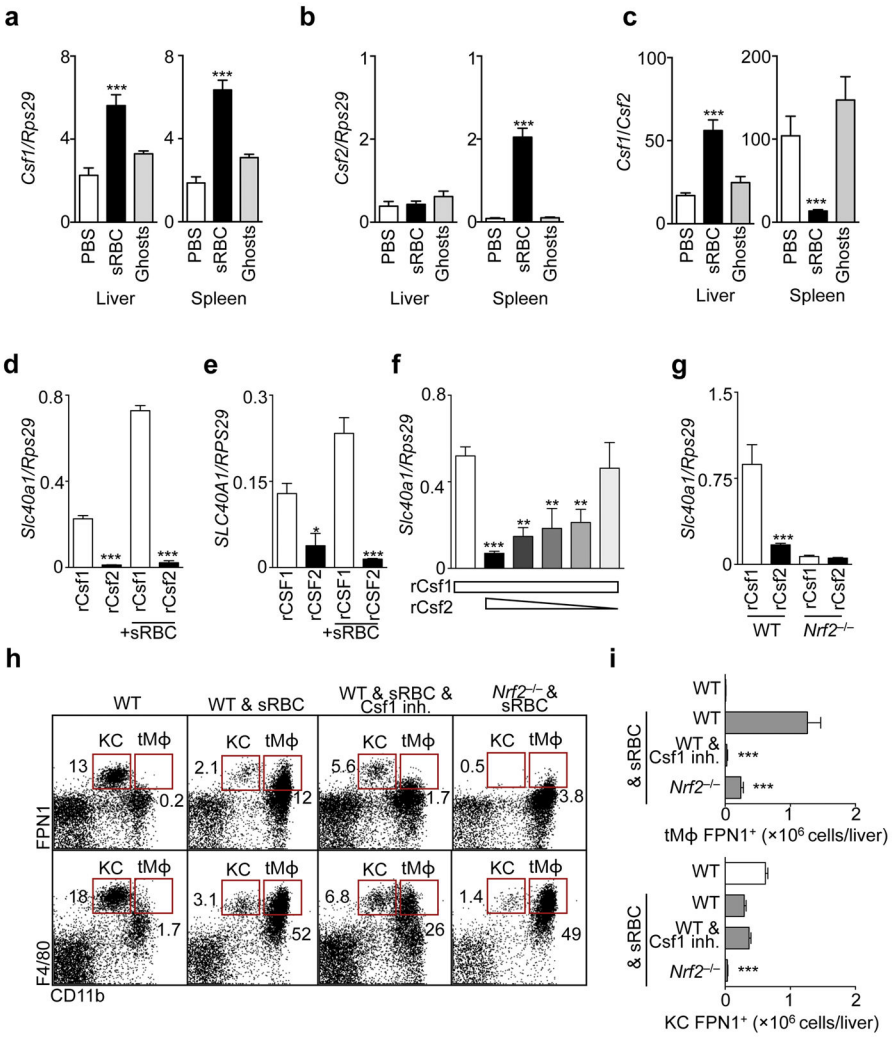

Figure 3. Csf1 and Nrf2 are essential to FPN1^{+} macrophage generation

(a) *Csf1*, (**b**) *Csf2* mRNA expression, and (**c**) the ratio of *Csf1* to *Csf2* in liver and spleen in steady state and 6 h after challenge with either sRBC, ghosts or PBS control. Means ± SEM; [n = 8 control and sRBC, n = 6 ghosts; ***P < 0.001 Kruskal-Wallis and Dunn's Multiple Comparison Test comparing all groups to controls]. (**d**) *Slc40a1* mRNA expression on mouse Ly-6C^{high} monocytes cultured with recombinant (r) Csf1, rCsf2, and sRBC. Means ± SEM; [n = 3 per group; *** P < 0.001 unpaired two-tailed t-test comparing Csf1 and Csf2-incubated monocytes for each condition]. Rps29 is the housekeeping gene. (**e**) *SLC40A1* mRNA expression on human CD14^{high} CD16^{-} monocytes cultured with rCSF1, rCSF2, and sRBC. Means ± SEM;; [n = 6 per group; ***P < 0.001 Anova Bonferroni's Multiple Comparison test comparing Csf1 and Csf2-incubated monocytes for each condition]. (**f**) *Slc40a1* mRNA expression on Ly-6C^{high} monocytes cultured with rCsf1 and decreasing doses of rCsf2, with sRBC. Means ± SEM; [n = 5 per group, except Csf2 0.01 ng/ml group, n = 3; *** P < 0.001, **P < 0.01 compared to rCsf1-cultured monocytes; Anova and Dunnett's Multiple Comparison Test]. (**g**) *Slc40a1* mRNA expression on mouse Ly-6C^{high} monocytes sorted from WT and *Nrf2*$^{-/-}$ mice and cultured with rCsf, rCsf2, and sRBC.

Means ± SEM, ***$P \leq 0.001$ compared to rCsf1-cultured monocytes for the same strain; Mann Whitney U test ($n = 5$ per group, except $Nrf2^{-/-}$ Csf2 group, $n = 4$). (**h**) Representative dot blots (1 of 3 experiments) and (**i**) quantification of KC and tMΦ in liver of WT mice in the steady state (white bars), and 16 h after sRBC challenge in WT mice, WT mice treated with the c-fms tyrosine kinase inhibitor Ki20227 (Csf1 inh.) and $Nrf2^{-/-}$ mice (grey bars). Means ± SEM; [$n = 3$ for WT control, WT sRBC, and WT sRBC/Ki20227; $n = 4$ for $Nrf2^{-/-}$ sRBC; ***$P < 0.001$ compared to sRBC-challenged WT mice; Anova Bonferroni's Multiple Comparison test].

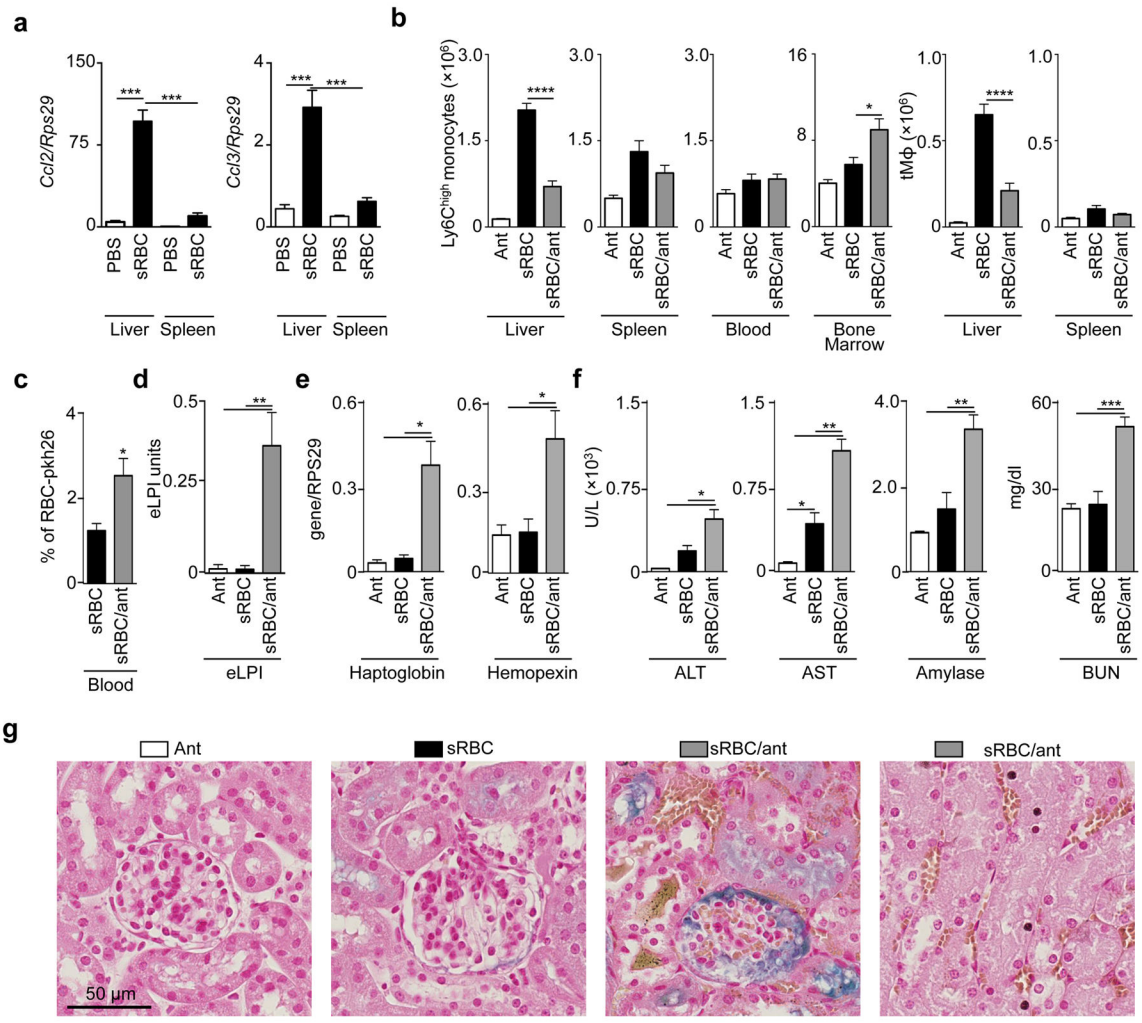

Figure 4. The on-demand mechanism preserves homeostasis

(**a**) *Ccl2* (left) and *Ccl3* (right) mRNA levels in the liver and spleen in response to sRBC or PBS. Means ± SEM; [$n = 6$ per group; ***$P < 0.001$; Anova Bonferroni's Multiple Comparison test]. (**b**) Quantification showing the effect of Ccr2 and Ccr5 antagonists (ant) on Ly-6C^{high} monocyte and tMΦ numbers in liver, spleen, blood, and bone marrow 16 h after sRBC challenge. Means ± SEM; [$n = 10$ Ant, $n = 9$ (sRBC bone marrow), $n = 10$ (sRBC/ant bone marrow), $n = 14$ all other groups (liver, spleen, blood); ****$P < 0.0001$, ***$P < 0.001$, **$P < 0.01$, and * $P < 0.05$; Anova Bonferroni's Multiple Comparison test]. (**c**) Quantification showing the effect of Ccr2 and Ccr5 antagonist treatment on pkh26^{+} Ter119^{+} CD45^{-} cell retention, as a fraction of the entire erythrocyte pool in the circulation 16 h after sRBC challenge. Means ± SEM; [$n = 4$ per group; *$P < 0.05$; Mann-Whitney U test]. (**d**) Effect of Ccr2 and Ccr5 antagonists (ant) on enhanced labile plasma iron (eLPI) levels in mice challenged with sRBC or controls. Means ± SEM; [$n = 8$ Ant, $n = 9$ sRBC, $n = 7$ sRBC/Ant; ** $P < 0.001$; Anova Bonferroni's Multiple Comparison test]. (**e**) Effect of Ccr2 and Ccr5 antagonists (Ant) on hemopexin and haptoglobin mRNA levels in the livers of mice challenged with sRBC or controls. Means ± SEM; [$n = 4$ per group; * $P < 0.05$; Anova Bonferroni's Multiple Comparison test]. (**f**) Effect of Ccr2 and Ccr5 antagonists

(Ant) on liver transaminase ALT, AST, Amylase, and blood urea nitrogen (BUN) activities and levels in serum 16 h after sRBC challenge. Means ± SEM; [$n = 4$ per group; *$P < 0.05$, **$P < 0.01$, and ***$P < 0.001$; Anova Bonferroni's Multiple Comparison test]. (**g**) Prussian blue staining on kidneys (nephron) from the three groups listed above. Iron depositions appear in blue, hemosiderin appears brown.